Neuroinformatics

1539-2791/05/49–64/$30.00

Original Article

A Modeling Environment With Three-Dimensional Morphology, A-Cell-3D, and Ca^{2+} Dynamics in a Spine

*Kazuhisa Ichikawa**

Human Information Systems Laboratories, Kanazawa Institute of Technology, Advanced Research Institute for Science and Engineering, Waseda University, 3-1 Yatsukaho Hakusan Kanazawa, 924-0838 Japan

Abstract

A-Cell-3D was developed to model and simulate a neuron with three-dimensional (3D) morphology utilizing graphic user interface (GUI)-based operations. A-Cell-3D generates and compartmentalizes 3D morphologies of a whole cell or a part of a cell based on a small number of parameters. A-Cell-3D has functions for embedding biochemical reactions and electrical equivalent circuits in the generated 3D morphology, automatically generating a simulation program for spatiotemporal numerical integration, and for visualizing the simulation results. A-Cell-3D is a free software and will be a powerful tool for both experimental and theoretical researchers in modeling and simulating neurons.

The Ca^{2+} dynamics in a dendritic spine and its parent dendrite were modeled and simulated to demonstrate the capabilities of A-Cell-3D. The constructed reaction-diffusion model comprised Ca^{2+} entry at the spine head, Ca^{2+} buffering by endogenous buffers, Ca^{2+} extrusion, and Ca^{2+} diffusion with or without exogenous Ca^{2+} indicator dyes. A simulation program was generated by A-Cell-3D, and differential equations were numerically integrated by the fourth-order Runge–Kutta method.

Index Entries: Modeling; simulation; morphology; reaction; diffusion; Hodgkin–Huxley equation; neuron; Ca^{2+} dynamics; spine.

Introduction

Signal transduction in a neuron occurs in the complex morphology of the dendrites, spines, axons, and cell body. The functions of a neuron emerge not only from complicated and complex biochemical reactions, but also from its unique three-dimensional (3D) morphology. Therefore, modeling and simulation of a neuron with its 3D morphology will provide important insight into neuronal function. There have been many

*Author to whom all correspondence and reprint requests should be addressed.
E-Mail: ichikawa@his.kanazawa-it.ac.jp

modeling and simulation studies on signal transduction in neurons (Lisman, 1989; Koch and Zador, 1993; Mell, 1993; De Schutter and Bower, 1994a,b; Ichikawa, 1994 and 1996; Dosemeci and Albers, 1996; Kamiyama et al., 1996; De Schutter. and Smolen, 1998; Bhalla and Iyengar, 1999; Volfovsky et al., 1999; Okamoto and Ichikawa, 2000). There are only a few models and simulations, however, that have investigated the effect of 3D morphology (Mell, 1993; Koch and Zador, 1993; Quandroni and Knopfel, 1994; De Schutter and Smolen, 1998; Volfovsky et al., 1999). The reason for this might be partly due to the difficult and time consuming work of constructing and programming the simulation of a biochemical reaction model with 3D morphology. Computer software to support the construction will aid modeling and simulation studies, and will be important for the advancement of computational neuroscience. Software of this kind is also important for neuroinformatics research (Usui, 2003). We developed a program called A-Cell-3D to produce a modeling and simulation environment for reaction-diffusion and electrical processes within the 3D morphology of a neuron.

A-Cell-3D was developed based on A-Cell, which is a free graphic user interface (GUI)-based software for modeling and simulating biochemical reactions (Ichikawa, 2001). A-Cell ignores the geometric properties of a neuron, and hence it is a modeling tool for a "single compartment." A-Cell-3D is an enhanced version of A-Cell enabling modeling and simulations in a 3D morphology. A-Cell-3D runs on the Windows operating system, and can be obtained by accessing its home page (http://www.his.kanagawa-it.ac.jp/~ichikawa).

Design and Functional Requirements

Basic Consideration and Design

Experimental researchers as well as theoreticians have the need to model and simulate neurons. In most cases, however, researchers are not experts in modeling and simulation and do not want to be concerned with simulation details. In addition, modeling and simulating complicated and complex neuronal systems are not easy, even for theoreticians. Therefore, an important consideration for the modeling tool is ease of use. The ease of use should be realized on three levels, model construction, simulation, and visualization of the results.

In the model construction stage, one method for describing a complicated 3D morphology is to divide it into many compartments and write a script that specifies the shape, size, and connectivity of each compartment. It is time consuming and laborious, however, to write such a script. In addition, it is almost impossible for researchers to determine the morphology described simply by reading the script. If the morphology is generated, viewed, and modified graphically as a 3D image, the above difficulties will be largely reduced and ease of use will be realized. In addition, embedding the biochemical reactions and Hodgkin–Huxley models in selected compartments should also be realized using the GUI. This avoids the time consuming and laborious work of designing a table to describe which models are embedded in which compartments. The use of such tables, however, makes it difficult to understand the spatial profile of the embedded models.

In the simulation stage, a computer program for spatiotemporal numerical integration should be automatically generated based on the constructed model, as in the existing modeling and simulation tools. This frees researchers from the laborious work of coding the simulation program. In addition, those who are not experts in computer programming can execute their own simulations.

In the visualization stage, the simulation results should be able to be viewed in various modes, including an animated display. A method for spatiotemporal analysis should also be realized with the GUI-based operation.

Simulation speed is also an important consideration. Approximately 10^{14} floating-point calculations are required for a 1-s-long simulation, if there are 10^4 compartments with 10^2 differential equations for each compartment and 10^2 arithmetic operations for each differential equation on average, and the simulation is performed with 10^{-6} s time steps. In general, a simulation program should be written so that its algorithm is easy to understand. This will, however, reduce the simulation speed. A-Cell-3D was developed not only for experts in computer programming and simulations, but also for nonexperts. Most researchers do not need to modify the generated simulation program. Therefore, calculation speed was prioritized over ease of understanding the simulation program.

The main memory size of a computer will limit the size of the model. If there are 10^4 compartments with 10^2 molecular species for each compartment and all these values are stored with double precision (8 bytes each) at 10^2 different time steps in the main memory, 800 MB are required. This main memory requirement is below the limitation of current personal computers. If the number of stored time steps is increased, however, the main memory requirement will exceed the present limits. Therefore, reduction of the main memory requirement is also an important consideration.

Functional Requirements

In the model construction stage, A-Cell-3D can (1) generate morphologies from a small number of input parameters, (2) automatically divide the morphologies into compartments, (3) embed biochemical and Hodgkin–Huxley models in selected compartments, (4) specify diffusion, and (5) specify boundary conditions. In the simulation stage, it can (1) automatically generate a simulation program from a graphically represented model and (2) specify initial conditions. Finally in the visualization stage, it can (1) display 3D simulation results with the capability of viewing inside the morphology, (2) produce an animated display, and (3) view the time-course and spatial profile.

Realizing Required Functions in A-Cell-3D

Generation of 3D Morphology

Generation of the complicated morphology of a neuron with minimum effort is difficult. One method is to generate the morphology from photographic data using the computer readable format employed in Virtual Cell (Schaff et al., 1997). This is a powerful tool for generating a realistic morphology. It is not always possible in modeling work, however, to obtain a photograph of desired morphology. Pre-preparation of several neuronal morphologies such as pyramidal, Purkinje, and stellate cells, however, often does not allow for generating a new morphology by modifying the pre-prepared morphology. Based on these considerations, A-Cell-3D generates a neuronal morphology using a generation algorithm (Tamori, 1993). By changing the parameters, a different neuronal morphology can be obtained. In addition, five morphologies, which are called "shapes" (cuboid, cylinder, sphere, cone, and spine/dendrite), are pre-prepared, and A-Cell-3D offers a means to generate new morphologies by combining these pre-prepared morphologies. The five pre-prepared morphologies and a resulting neuron shape are shown in Fig. 1A.

Cuboid, cylinder, sphere, and cone shapes can be used alone as a morphology representing a cell or parts of a cell. The spine/dendrite shape is pre-prepared because special interests are focused on this morphology. The method for generating these shapes is simple, and is realized by specifying a small number of parameters. The spine/dendrite shape can be

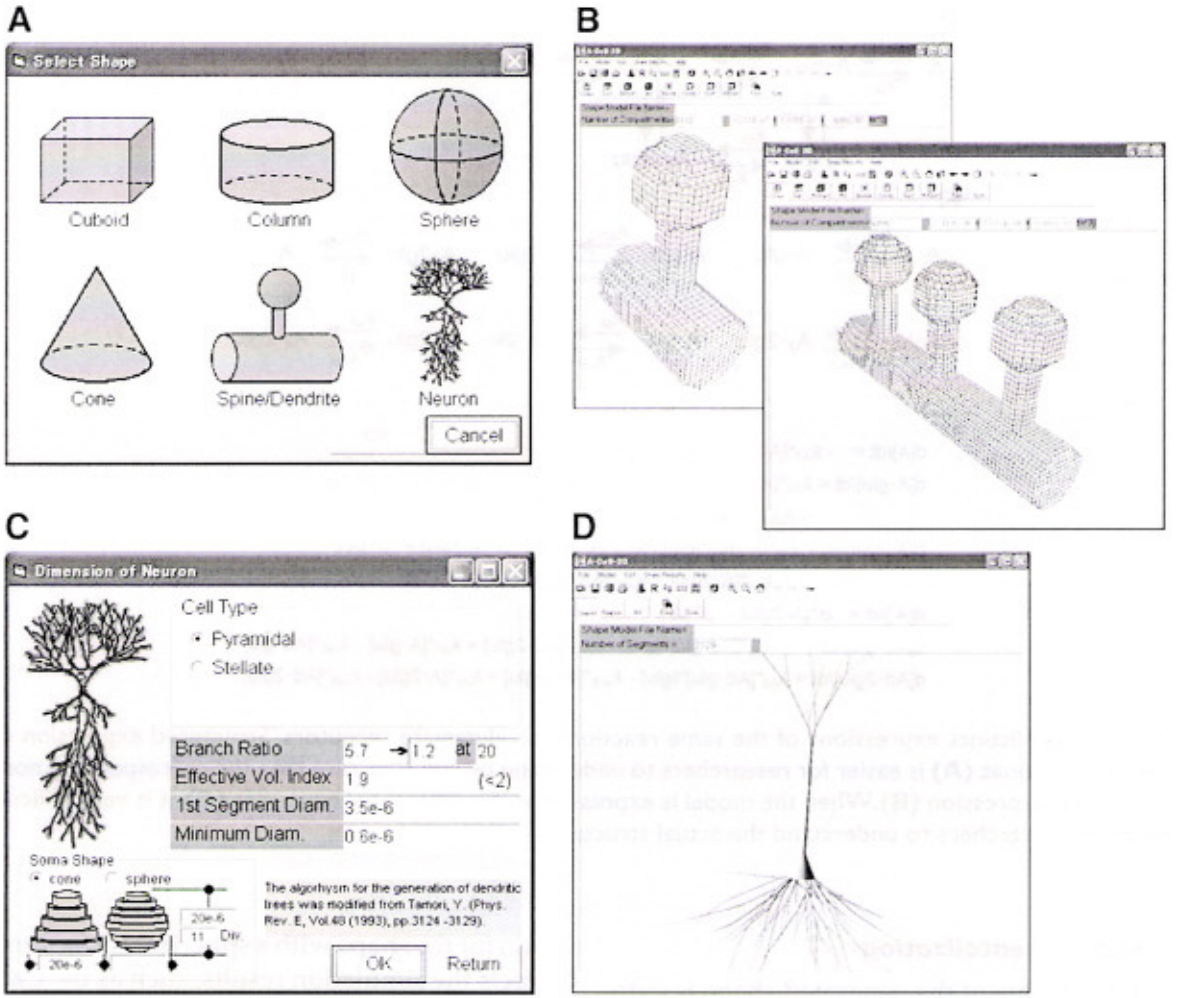

Fig. 1. Pre-prepared 3D morphologies in A-Cell-3D and examples of generated spine/dendrite and a neuron shape. A-Cell-3D has six pre-prepared 3D morphologies **(A)**. A single spine/dendrite or multiple spines with a parent dendrite can be generated **(B)**. A neuron shape is generated by specifying parameters **(C)**, and an example of a generated pyramidal cell is shown **(D)**.

generated by specifying six clearly defined parameters. Two examples of generated spine/dendrite shapes are shown in Fig. 1B. Multiple spines can be generated on the same dendrite, as shown in Fig. 1B. The neuron shape can be generated by specifying 11 parameters (Fig. 1C). An example of a generated pyramidal cell is shown in Fig. 1D.

A-Cell-3D has the capability to specify the membrane surface. This function is important for embedding membranous molecules such as glutamate receptor channels. A-Cell-3D automatically converts the surface density to the number of molecules on each membrane. Thus, there is no need for the user to calculate and specify this number for each membrane surface.

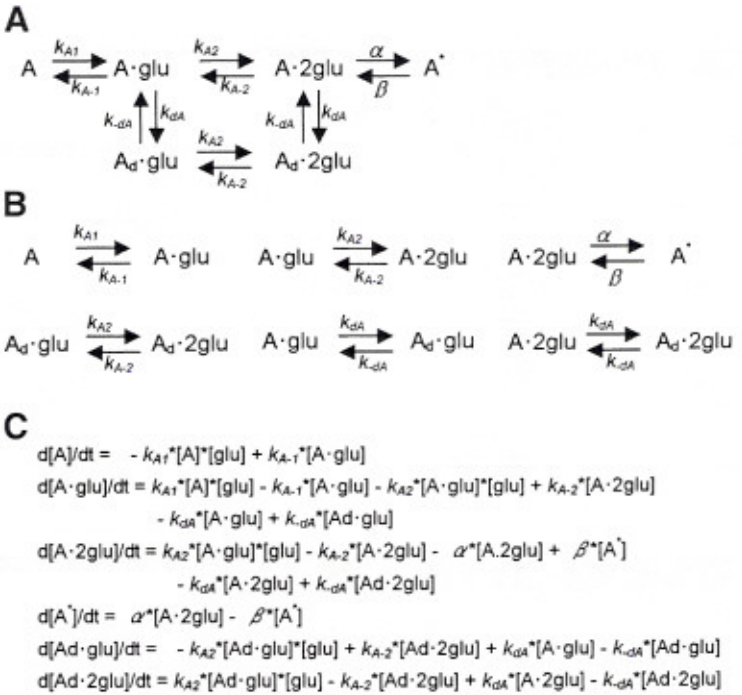

Fig. 2. Three distinct expressions of the same reactions for glutamate receptors. Structured expression of reaction schemes **(A)** is easier for researchers to understand overall structure than the corresponding non-structured expression **(B)**. When the model is expressed as the differential equations **(C)**, it is very difficult for most researchers to understand the actual structure.

Compartmentalization

The volume of the generated shape is automatically divided into equal-size cuboid compartments by A-Cell-3D based on the specified number of divisions. In the neuron shape, compartments are cylinders of various diameters and lengths according to their position on the dendritic tree. The cubic compartment was selected to optimize the calculation speed of the simulation. For a cubic compartment, the addresses of the adjacent six compartments can be obtained easily from the x, y, and z index numbers, by which the compartment is identified. This eliminates an address conversion process in the simulation program, and hence increases the calculation speed. Although this raises a problem of a bigger surface-to-volume ratio for the shape with a spherical surface and affects the simulation results, such as the Ca^{2+} dynamics by the inward flow via NMDA receptors, practical steps can be taken to avoid this problem (*see* Discussion).

Construction of Biochemical and Hodgkin–Huxley Models

A-Cell-3D has a function for constructing biochemical and Hodgkin–Huxley models, which is the same as A-Cell (Ichikawa, 2001). The model is easily constructed using GUI-based operations. Three different expressions of the same reactions for the binding of glutamate to AMPA receptors are shown in Fig. 2.

Figure 2A is a graphically expressed model. This is very advantageous, as it is easier to under-

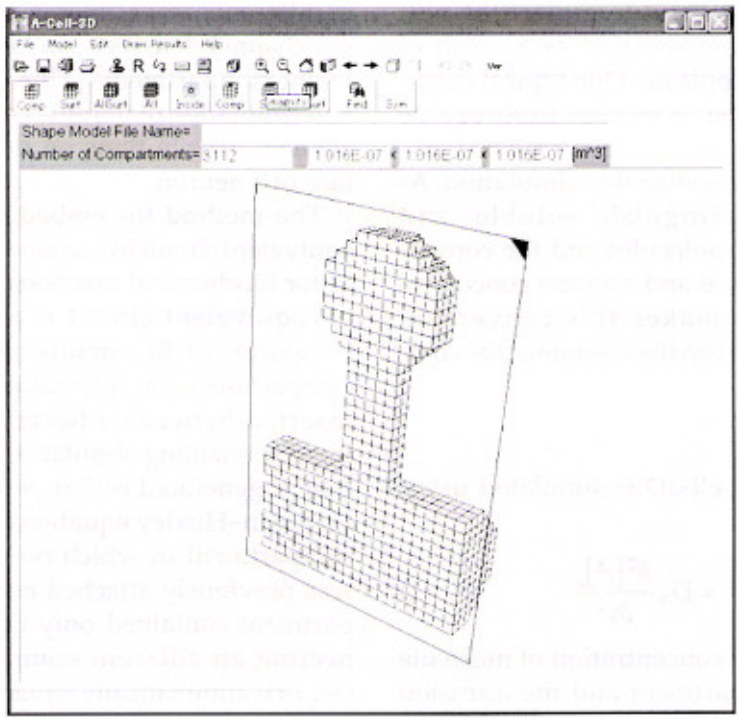

Fig. 3. Cross-section of the generated shape. The shape can be cross-sectioned by cutting it along the plane, as shown by a rectangle of the selected surface direction.

stand the overall structure of the reaction scheme. The same model can be expressed by a set of reactions as shown in Fig. 2B. This format facilitates the generation of differential equations by the computer program, but it is not easy for researchers to understand the overall structure. A model expressed by differential equations is shown in Fig. 2C. This form of expression is widely used in computational simulations, and the expressions shown in Figs. 2A,B are finally converted to the differential equations before simulation. Expression of the model using the form shown in Fig. 2A is essential for constructing complex and complicated models.

Attaching Biochemical Reactions to Compartments

The constructed biochemical reaction and Hodgkin–Huxley models should be embedded in the desired compartments. This process should be performed using GUI-based operation. To realize this, A-Cell-3D has several methods for specifying the compartments in which biochemical reactions are embedded. With these methods, reaction schemes can be embedded in selected single or multiple compartments, all compartments, and selected or all surface compartments. To embed reactions in compartments inside the shape, A-Cell-3D has the capability to generate a cross section of the shape, as shown in Fig. 3. The shape can be rotated, shifted, enlarged, and reduced to access any compartment in the shape. A-Cell-3D has the capability to view compartments embedded with specified reactions. This aids in viewing the location of embedded reactions in the 3D morphology.

Soluble and Membrane-Bound Molecules

In some cases, soluble molecules will be generated as a result of reactions on the membrane.

In addition, some soluble molecules will become membrane-associated as a result of reactions in the cytoplasm. One typical example is the generation of inositol triphosphate (soluble) by phospholipase C (membrane-bound protein). To realize this simulation, A-Cell-3D can distinguish soluble and membrane-bound molecules and the conversion between surface and volume concentrations. A-Cell-3D makes this conversion automatically based on the volume of the compartment.

Diffusion

Diffusion in A-Cell-3D is simulated using Fick's equation.

$$\frac{\delta[A]_i}{\delta t} = D_A \frac{\delta^2[A]_i}{\delta x^2} \quad (1)$$

$[A]_i$ and D_A are the concentration of molecule A in the i-th compartment and the diffusion coefficient, respectively. Instead, the calculation routine for diffusion is automatically inserted into the simulation program when diffusion is specified for the molecule.

Simulations for 1D diffusion were performed with a shape comprising 1 μm^3 cubic compartments. The diffusion coefficient was $10^{-10} m^2/s$. The simulations agreed well with the theory, confirming the correct simulation of diffusion using Fick's equation by A-Cell-3D (data not shown). Diffusions in the cytoplasm and on the membrane are differently calculated in the simulation program based on the soluble/membrane properties of the molecule.

Embedding Hodgkin–Huxley Models in Compartments

Generation of action potentials and their propagation in the 3D morphology is also modeled by A-Cell-3D. An embedded electrical equivalent circuit involves the combination of voltage-gated sodium channels, potassium channels, calcium channels, and so on. Different combinations can be embedded in different compartments. In addition, different channel densities can be specified for different compartments. This enables modeling and simulation of the effect of inhomogeneous channel distributions on the membrane surface of a neuron.

The method for embedding an electrical equivalent circuit in a compartment is the same as for biochemical reactions. When an electrical equivalent circuit is embedded to one compartment, RC circuits connecting adjacent compartments are automatically generated and inserted between adjacent compartments, thereby enabling simulations of the propagation of generated action potentials. If a set of Hodgkin–Huxley equations is embedded in a compartment in which no equivalent circuit was previously attached and hence the compartment contained only the RC circuit connecting an adjacent compartment, the RC circuit is automatically replaced by the attached equivalent circuit. An example of embedded Hodgkin–Huxley model and automatically inserted RC circuits are shown in Fig. 4.

In this example, S_i is a combination of voltage sensitive channels, leakage conductance, and other conductance, together with the membrane capacitance. The simulation results by A-Cell-3D replicated published results (Koch, 1999) confirming the validity of the modeling and simulation of Hodgkin–Huxley model (data not shown).

Boundary Conditions

When only a part of the morphology of a neuron is modeled, there are open ends. One such example occurs with the spine/dendrite shape, where the dendrite is truncated at two positions as shown in Fig. 1B. In this case, boundary conditions should be specified at these open ends. In A-Cell-3D, the open ends can be connected to a fixed concentration of a large reservoir, eliminating the buildup of molecules within the shape. This is realized by embedding reactions and equations in

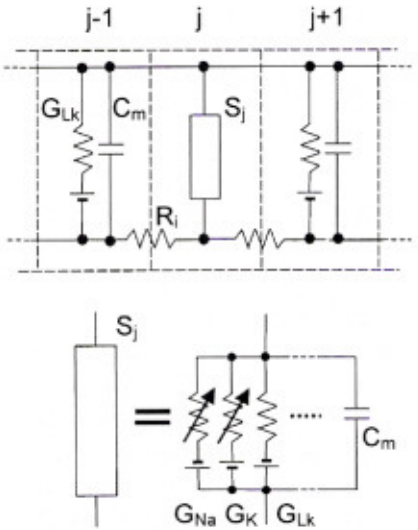

Fig. 4. Electrical equivalent circuit used in A-Cell-3D. When an electrical equivalent circuit, which contains voltage sensitive channels, is embedded in a compartment, the RC circuit is automatically inserted in all compartments to simulate the propagation of generated action potentials.

compartments at the truncated surfaces. For the propagation of action potentials, the open ends can be connected to an electrical equivalent circuit representing the rest of the neuron.

Simulation Program

The simulation program is generated automatically by A-Cell-3D based on the constructed 3D model. The fourth-order Runge–Kutta method with a fixed time step was used for the numerical integration of generated differential equations. The simulation program has calculation loops for the *x*-, *y*-, and *z*-axes selecting compartments within a loop for each time step, thereby enabling spatiotemporal integration. At the beginning of each calculation time step, the simulation program saves the current values for all variables of all compartments, and then begins calculations to obtain new variable values for each compartment one at a time until all compartment values are calculated. After this, all variable values of all compartments are updated and the next calculation time step begins. Thus, the updating of variable values is performed synchronously for all compartments.

The generated simulation program is written in C language. To optimize calculation speed, the generated simulation program uses a limited number of C language function calls. This increases the calculation speed markedly. Although this programming method reduces the readability and modifiability of the programming code, we prioritized the simulation speed (*see* Design and Functional Requirements section).

After compilation, the simulation is started by executing the program. The calculation results are stored as a binary disk file to reduce disk space requirements; the file will be read by A-Cell-3D for viewing the results.

Initial Conditions

The initial values of the variables are stored as a disk file together with the calculation time step. The generated simulation program reads this disk file at the beginning of the simulation. Thus, the initial condition data and the simulation program are stored as independent files, and the same simulation program can be used for different simulations having different initial conditions.

A-Cell-3D has a function for selecting output variables. To reduce the memory requirement, the variables of interest can be viewed selectively.

Viewing and Analysis of Simulation Results

The software should provide various means for viewing and analyzing simulated results. A-Cell-3D has functions for viewing results serially by time and as an animation. Values of a selected parameter are displayed in pseudocolor. The inside of the shape can be seen as cross-sections of the shape.

Time-course drawing (temporal profile) of selected molecules in any single compartment,

and spatial profile drawing of selected molecules along a specified line enables further analysis. The numerical values can be read along these profiles. Calculated results are exported to a text file, and can be imported by other software for further analysis.

Modeling and Simulation of Ca^{2+} Dynamics in a Spine

We constructed a model for Ca^{2+} dynamics in a dendritic spine and its parent dendrite as an example of an application using A-Cell-3D. The simulation results showed the localized distribution of Ca^{2+} within the spine as reported in experimental observations (Segal et al., 2000; Goldberg et al., 2003). By changing the initial conditions of the simulation, which involved inclusion or exclusion of the intrinsic calcium buffers and extrusion system, intrinsic buffer diffusion, type of indicator dye and its concentration, the distribution of Ca^{2+} within a spine was largely changed. The results of simulations in which indicator dyes are used require careful interpretation, and further simulations are needed to obtain the comprehensive results.

Model

The 3D morphology used in the present model is shown in Fig. 5. The diameter of the spine head was 0.5 µm. The diameter and length of the spine neck were 0.2 µm and 0.4 µm, respectively. The diameter of the parent dendrite was 0.5 µm, and the length was 10 µm to avoid the effect of truncation in the model dendrite. The spine/dendrite shape had 22,276 compartments. Dark compartments (shown in red in A-Cell-3D) in Fig. 5 indicate those to which the reactions shown below the shapes are attached. A model for inward Ca^{2+} flux was embedded in the top of the spine head, Ca^{2+} leakage and extrusion were on the membrane surface, and Ca^{2+} buffers and indicator dye were in all compartments. The rectangle in Fig. 5 indicates the plane by which the spine/dendrite shape is cut to show the inside of the dendrite.

Ca^{2+} entry was modeled by a double-exponential function simulating the desensitization of NMDA receptors. The duration of the stimulation was 1 s, assuming a tetanic stimulation for the induction of long-term potentiation. The peak Ca^{2+} current through a spine was estimated to be 0.6 pA, assuming that NMDA receptor current in a single spine of 6 pA and that 10% of this current is carried by Ca^{2+} (De Schutter and Bower, 1993; Burnashev et al., 1995; Rogers et al., 1995). In the present simulation, the peak Ca^{2+} current through the spine was 0.603 pA. Medium and low affinity Ca^{2+} buffers were used in the model. These buffers were diffusing or stationary, depending on the initial condition of the simulations. In the resting state, Ca^{2+} leakage was balanced by Ca^{2+} extrusion via the extrusion system, which is modeled with a Michaelis–Menten type reaction scheme. The reaction between Ca^{2+} and the indicator dye was expressed by a bi-directional reaction. Fura-2 and fluo-4 were selected for the simulation as slow and fast kinetic indicator dyes, respectively. Diffusion constants for Ca^{2+} and the Ca^{2+} indicator dyes were all $10^{-10} m^2/s$, while those for endogenous buffers were $10^{-11} m^2/s$ (Allbritton et al., 1992; Zhou and Neher, 1993; Gabso et al., 1997).

A Ca^{2+} indicator dye was included in the model to examine the extent to which spatiotemporal characteristics of the intracellular Ca^{2+} concentration ($[Ca^{2+}]_i$) was accurately estimated. The estimated Ca^{2+} concentration ($[Ca^{2+}]_e$) was calculated by the following equation, which simulates the fluorescence measurements.

$$[Ca^{2+}]_e = (k_{-D}/k_D) \times [\text{DyeCa}]/[\text{Dye}] \qquad (2)$$

k_D and k_{-D} are the forward and backward rate constants for the binding between Ca^{2+} and the indicator dye. [DyeCa] and [Dye] are concentrations of Ca^{2+}-bound and Ca^{2+}-free dye, respectively. The total dye concentration varied from 10 to 200 μM. Values for k_D (1×10^8 $/M/s$ and 6×10^8 $/M/s$ for fura-2 and fluo-4, respectively)

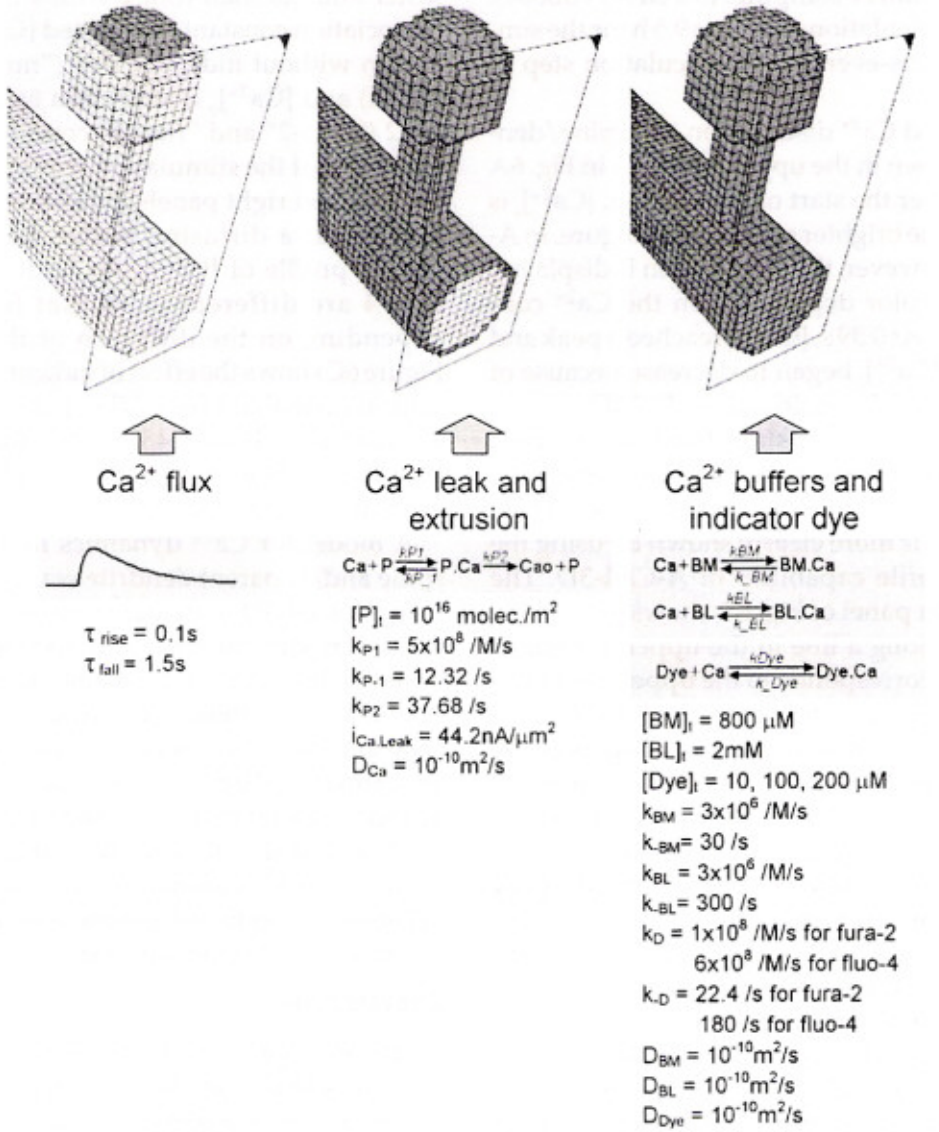

Fig. 5. A 3D model for the Ca^{2+} dynamics in a spine/dendrite shape. The diameter of the spine head was 0.5 μm. The diameter and length of the spine neck were 0.2 μm and 0.4 μm, respectively. The diameter of the parent dendrite was 0.5 μm, and the length was 10 μm. Dark compartments indicate those in which the corresponding reactions are embedded. Rectangles indicate planes by which the spine/dendrite shape is cut to show the inside of the dendrite.

and k_{-D} (22.4 /s and 180 /s for fura-2 and fluo-4, respectively) were obtained from published articles (Connor et al., 1980; Sinha et al., 1997; Maravall et al., 2000).

Simulation Results

Automatically generated simulation program was compiled and run by Microsoft VC++6.0 on Windows XP Pro Service Pack 2

using Pentium IV computer (3.2 GHz/FSB800). The total calculation time was 9.5 h for the simulation of 2 s-events with calculation step of 2×10^{-6} s.

Simulated Ca^{2+} distribution in a spine/dendrite is shown in the upper left panel in Fig. 6A at 0.39 s after the start of stimulation. $[Ca^{2+}]_i$ is higher in the brighter region in this figure. In A-Cell-3D, however, the distribution is displayed in pseudocolor depending on the Ca^{2+} concentration. At 0.39 s, $[Ca^{2+}]_i$ reached a peak and after this $[Ca^{2+}]_i$ began to decrease because of the simulated desensitization of NMDA receptors. Localized Ca^{2+} distribution within a spine is visualized as was reported in experimental observations (Segal et al., 2000; Goldberg et al., 2003). This is more clearly shown by using the spatial profile capability of A-Cell-3D. The upper right panel of Fig. 6A shows $[Ca^{2+}]_i$ distribution along a line in the upper left panel. Position 0 corresponds to the uppermost compartment in the spine head. The lowest curve is the spatial profile in the case where both the extrusion system and buffers are included in the simulation (+Extr/+Buff). $[Ca^{2+}]_i$ decays monotonically toward the spine neck. When buffers were excluded (+Extr/−Buff), the peak $[Ca^{2+}]_i$ increased a little. The change in the distribution, however, was small. When the extrusion system was excluded (−Extr/+Buff), the curve shifted upward, and there was an increase in $[Ca^{2+}]_i$ in the parent dendrite. The time-course of $[Ca^{2+}]_i$ at the compartment indicated by the box in the lower left panel in Fig. 6A is shown in the lower right panel using the time-course drawing capability of A-Cell-3D. By excluding or including the extrusion system and buffers in the simulation, it was apparent that the extrusion system reduced the peak $[Ca^{2+}]_i$ (comparison between +Extr/+Buff and −Extr/+Buff), while the buffers shifted the time to peak to the left (comparison between +Extr/+Buff and +Extr/−Buff).

The effects of the indicator dye are shown in Figs. 6B,C. Fluo-4 has approximately six times faster kinetics than fura-2 with a comparable dissociation constant. Simulated $[Ca^{2+}]_i$ distribution without indicator dye ("no dye" condition) and $[Ca^{2+}]_e$ distribution calculated by eq. 2 ("fura-2" and "fluo-4" conditions) at 1 s after start of the stimulation are shown in Fig. 6B. Left and right panels indicate a stationary buffer and a diffusing buffer, respectively. Spatial profile of $[Ca^{2+}]_e$ for both fura-2 and fluo-4 are different from that for $[Ca^{2+}]_i$, depending on the diffusion of the buffers. Figure 6C shows the effect of indicator dye concentration both for fura-2 (left panel) and fluo-4 (right panel) at 0.45 s after the start of stimulation. Fluo-4 (10 μM) gave a fairly good estimation of the spatial profile.

A model for Ca^{2+} dynamics in a dendritic spine and its parent dendrite was constructed using A-Cell-3D to demonstrate its capability for 3D model construction and simulation based on biochemical reactions and diffusion. A-Cell-3D also offers several display and analysis types like time-course, spatial profile, and an animated display, which cannot be adequately presented in a paper article. Estimated Ca^{2+} spatial distribution with indicator dye changed under various conditions, as shown in Fig. 6. Further investigation is needed to clarify the effect of indicator dyes.

Discussion

We developed a tool, A-Cell-3D, for modeling and simulating the 3D morphology of a whole neuron or a part of a neuron. A-Cell-3D is free GUI-based software for both experimental and theoretical researchers. A model of Ca^{2+} dynamics in a spine using A-Cell-3D was constructed and simulation results were shown as an example of A-Cell-3D application. The GUI-operation of A-Cell-3D will facilitate modeling studies by both experimental and theoretical researchers. Existing software packages for modeling 3D morphology were not used in A-Cell-3D, so that A-Cell-3D can be further developed, e.g., changes in the morphology

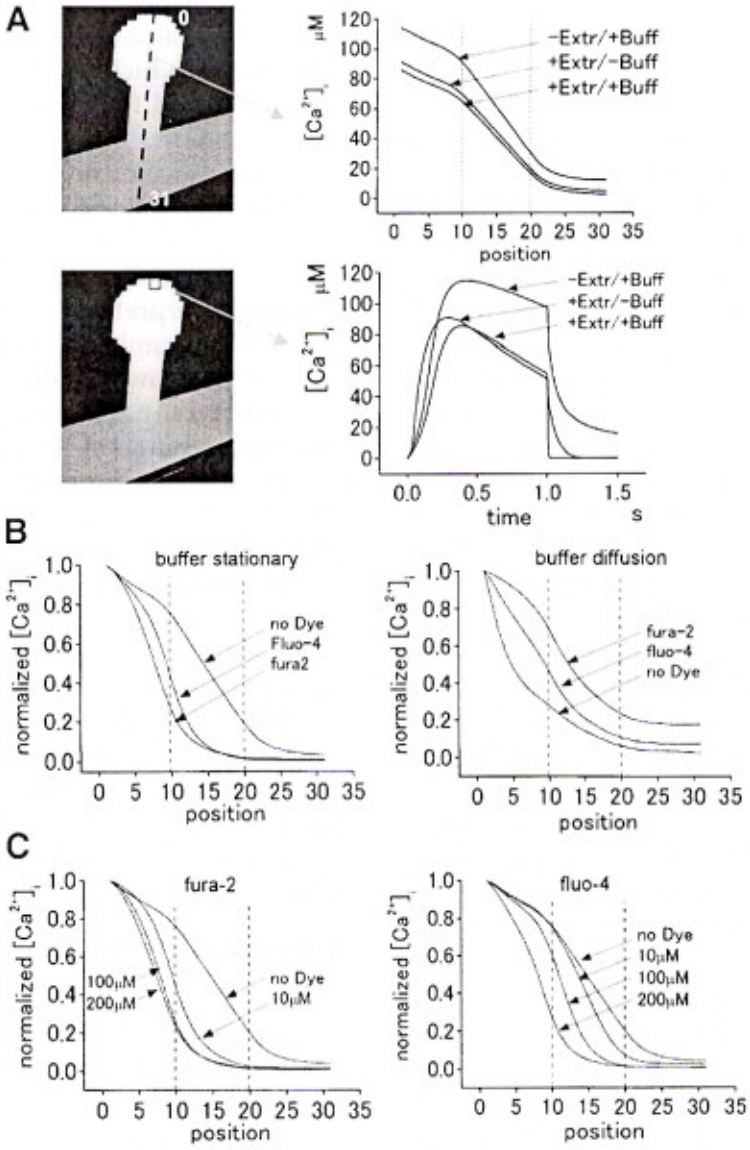

Fig. 6. Simulation results of the model. Spatial distribution of Ca^{2+} at 0.39 s after the start of stimulation is shown in the upper panel. $[Ca^{2+}]_i$ is higher in the brighter region. The increase in $[Ca^{2+}]_i$ is confined in the spine head and neck. Spatial profiles along the dashed line under several conditions of excluding or including the extrusion system (−Extr or +Extr) and buffers (−Buff or +Buff) are drawn. In the presence of the Ca^{2+} extrusion (+Extr), the spatial distribution of Ca^{2+} is reduced almost within the spine head and the neck. Two vertical broken lines indicate the positions of the head-neck and neck-dendrite boundaries. The time-course at the compartment indicated by the rectangle is shown in the lower panel. The extrusion system contributes to the reduction in the peak $[Ca^{2+}]_i$, while buffers contribute to the $[Ca^{2+}]_i$ kinetics **(A)**. The estimated Ca^{2+} concentration, $[Ca^{2+}]_e$, by simulating fluorescent measurements using fura-2 and fluo-4 show different results, depending on the buffer diffusion or stationary condition **(B)**. $[Ca^{2+}]_e$ dependence on the concentration of indicator dyes. Fluo-4 (10 μM) gives fairly good estimation in the present simulation condition **(C)**.

during a simulation, generation of new intracellular organelles from soluble materials, and cell division.

The shape of compartments used in A-Cell-3D is cuboid. This means that a spherical surface is not well approximated and raises the problem of the surface-to-volume ratio. For example, if a sphere is divided into equal-sized cubic compartments giving the same volume as the original sphere, the surface area with the cubic compartments is approx 45% higher than that of the original sphere. If the embedded molecule has a dimension of surface density, such as the leakage Ca^{2+} current, the total Ca^{2+} leakage current over the entire surface will be 45% larger than that through the original spherical surface. This will cause higher $[Ca^{2+}]_i$ than expected. This can be avoided, however, by setting the surface leakage density to a 45% smaller value. This results in the same total Ca^{2+} leakage current as from the original surface.

It is possible to cover the spherical surface with triangle planes to obtain a smoother surface and reduce the error in the surface-to-volume ratio. This means that the simulation program would have to distinguish between two different compartments having different shapes and volumes. This will reduce the calculation speed. In the present version of A-Cell-3D, therefore, the shape (cube) and size of all the compartments are the same to avoid reducing the calculation speed.

Intracellular organelles are apparatuses within a cell, and include the endoplasmic reticulum, mitochondria, nucleolus, cytoskeleton, and so on. Experimental data for these apparatuses are accumulating and the importance for simulating these has been recognized (Fischer et al., 1998; Majewska et al., 2000; Lamprecht and LeDoux, 2004; Yuste and Bonhoeffer, 2004). The present version of A-Cell-3D, however, does not model these intracellular organelles. Soon A-Cell-3D will include a function for modeling and simulating intracellular organelles. The modeling and simulation of the extracellular environment of the neuron is also being developed.

In cases in which the molecular concentration is low and the volume of the compartment is small, only a small number of molecules exist within a compartment. In this case, the calculation of molecular concentration using differential equations is inadequate, and the simulation results must be carefully interpreted. If we assume that the law of large numbers holds in Ca^{2+} dynamics in a spine, however, the calculation results using differential equations provides an ensemble average of the molecular concentration, and still offers useful information. An alternative approach under conditions of small number of molecules is stochastic simulation using Monte Carlo methods (Stiles and Bartol, 2000).

The simulation results for Ca^{2+} dynamics in the spine/dendrite shape indicated that the rise in $[Ca^{2+}]_i$ in the dendrite is very small in comparison to that in the spine. Similar simulation results were previously reported (Volfovsky et al., 1999). Further simulations will provide insight into Ca^{2+} dynamics in a spine.

Acknowledgments

This study was partly supported by Special Coordination Funds of the Science and Technology Agency of the Japanese Government. The author thanks Mr. Yoda of Logistics, Inc. for the programming of A-Cell-3D.

References

Allbritton, N. L., Meyer, T., and Stryer, L. (1992) Range of messenger action of calcium ion and inositol 1,4,5-triphosphate. Science 258, 1812–1815.

Bhalla, U. S. and Iyengar, R. (1999) Emergent properties of networks of biological signaling pathways. Science 283, 381–387.

Burnashev, N., Zhou, Z., and Neher, E. (1995) Fractional calcium currents through recombinant GluR channels of the NMDA, AMPA and kainate receptor subtypes. J. Physiol. 485, 403–418.

Connor, J. A., Wadman, W. J., Hockberger, P. E., and Wong, R. K. S. (1988) Sustained dendritic gradients of Ca^{2+} induced by excitatory amino acids in CA1 hippocampal neurons. Science 240, 649–653.

De Schutter, E. and Bower, J. M. (1993) Sensitivity of synaptic plasticity to the Ca^{2+} permeability of NMDA channels: a model of long-term potentiation in hippocampal neurons. Neural Comp. 5, 681–694.

De Schutter, E. and Bower, J. M. (1994a) An active membrane model of the cerebellar Purkinje cell. I. Simulation of current clamps in slice. J. Neurophysiol. 71, 375–400.

De Schutter, E. and Bower, J. M. (1994b) An active membrane model of the cerebellar Purkinje cell II. Simulation of synaptic responses. J. Neurophysiol. 71, 401–419.

De Schutter, E. and Smolen, P. (1998) Calcium dynamics in large neuronal models. In: Methods in Neuronal Modeling, 2nd edn. Koch, C. and Segev, I. (eds.) The MIT Press, Cambridge, MA, pp.211–250.

Dosemeci, A. and Albers, R. W. (1996) A mechanism for synaptic frequency detection through autophosphorylation of Cam kinase II. Biophys. J. 70, 2493–2501.

Fischer, M., Kaech, S., Knutti, D., and Matus, A. (1998) Rapid actin-based plasticity in dendritic spines. Neuron 20, 847–854.

Gabso, M., Neher, E., and Spira, M. E. (1997) Low mobility of the Ca^{2+} buffers in axons of cultured Aplysia neurons. Neuron 18, 473–481.

Goldberg, J. H., Tamas, G., Aronov, D., and Yuste, R. (2003) Calcium microdomains in aspiny dendrites. Neuron 40, 807–821.

Ichikawa, K. (1994) Transduction steps which characterize retinal cone photocurrent induced by flash stimuli. Neurosci. Res. 20, 337–343.

Ichikawa, K. (1996) Modeling and analysis of spatio-temporal change in $[Ca^{2+}]_i$ in a retinal rod outer segment. Neurosci. Res. 25, 137–144.

Ichikawa, K. (2001) A-Cell: graphical user interface for the construction of biochemical reaction models. Bioinformatics 17, 483–484.

Kamiyama, Y., Ogura, T., and Usui S. (1996) Ionic current model of the vertebrate rod photoreceptor. Vis. Res. 36, 4059–4068.

Koch, C. and Zador, A. (1993) The function of dendritic spines: devices subserving biochemical rather that electrical compartmentalization. J. Neurosci. 13, 413–422.

Koch, C. (1999) Biophysics of Computation. Oxford University Press, New York.

Lamprecht, R. and LeDoux, J. (2004) Structural plasticity and memory. Nat. Rev. Neurosci. 5, 45–54.

Lisman, J.E. (1989) A mechanism for the Hebb and the anti-Hebb processes underlying learning and memory. Proc. Natl. Acad. Sci. USA 86, 9574–9578.

Majewska, A., Tashiro, A., and Yuste, R. (2000) Regulation of spine calcium dynamics by rapid spine motility. J. Neurosci. 20, 8262–8268.

Maravall, M., Mainen, Z. F., Sabatini, B. L., and Svoboda, K. (2000) Estimating intracellular calcium concentrations and buffering without wavelength ratioing. Biophys. J. 78, 2655–2667.

Mell, B. W. (1993) Synaptic integration in an excitable dendritic tree. J. Neurophysiol. 70, 1086–1101.

Okamoto, H. and Ichikawa, K. (2000) Switching characteristics of a model for biochemical-reaction network describing autophosphorylation versus dephosphorylation of Ca^{2+}/calmodulin-dependent protein kinase II. Bio. Cyber. 82, 35–47.

Quandroni, R. and Knopfel, T. (1994) Compartmental models of type A and type B guinea pig medial vestibular neurons. J. Neurophysiol. 72, 1911–1924.

Rogers, M., Dani, J. A., and Nozawa, M. (1995) Comparison of quantitative calcium flux through NMDA, ATP, and ACh receptor channels. Biophys. J. 68, 501–506.

Schaff, J., Fink, C. C., Slepchenko, B., Carson, J. H., and Loew, L. M. (1997) A general computational framework for modeling cellular structure and function. Biophys. J. 73, 1135–1146.

Segal, M., Korkotian, E., and Murphy, D. D. (2000) Dendritic spine formation and pruning: common cellular mechanisms? TINS 23, 53–57.

Sinha, S. R., Wu, L. G., and Saggau, P. (1997) Presynaptic calcium dynamics and transmitter release evoked by single action potentials at mammalian central synapses. Biophys. J. 72, 637–651.

Stiles, J. R. and Bartol, T. M. (2000) Monte Carlo methods for simulating realistic synaptic microphysiology using Mcell. In: Computational Neuroscience: Realistic Modeling for Experimentalists. De Schutter, E. (ed.) CRC Press, Boca Raton, FL, pp. 87–127.

Tamori, Y. (1993) Theory of dendritic morphology. Phys. Rev. E. 48, 3124–3129.

Usui, S. (2003) Visiome: neuroinformatics research in vision project. Neural Netw. 16, 1293–1300.

Volfovsky, N., Parnas, H., Segal, M., and Korkotian, E. (1999) Geometry of dendritic spines affects calcium dynamics in hippocampal neurons: theory and experiments. J. Neurophysiol. 81, 450–462.

Yuste, R. and Bonhoeffer, T. (2004) Genesis of dendritic spines: insight from ultrastructural and imaging studies. Nat. Rev. Neurosci. 5, 24–34.

Zhou, Z. and Neher, E. (1993) Mobile and immobile calcium buffers in bovine adrenal chromaffin cells. J. Physiol. 469, 245–273.